A cyclone climatology of the British-Irish Isles 1871-2012

Matthews[1] T, Murphy[2] C, Wilby[3] RL, Harrigan[2] S

[1] School of Natural Sciences and Psychology, Liverpool John Moores University, UK

[2] ICARUS, Department of Geography, National University of Ireland Maynooth, Republic of Ireland

[3]Department of Geography, Loughborough University, UK

Abstract

The British-Irish Isles (BI) lie beneath the North Atlantic storm track year-round and thus are impacted by the passage of extra-tropical cyclones. Given recent extreme storminess and projections of enhanced winter cyclone activity for this region, there is much interest in assessing the extent to which the cyclone climate of the region may be changing. We address this by assessing a 142-year (1871-2012) record of cyclone frequency, intensity and 'storminess' derived from the 20CR dataset. We also use this long-term record to examine associations between cyclone activity and regional hydroclimate. Our results confirm the importance of cyclone frequency in driving seasonal precipitation totals which we find to be greatest during summer months. Cyclone *frequency* and *storminess* are characterised by pronounced inter-annual and multi-decadal variability which are strongly coupled to atmospheric blocking in the Euro-Atlantic region, but we detect no evidence of an increasing trend. We observe an upward trend in cyclone *intensity* for the BI region, which is strongest in winter and consistent with model projections, but promote caution interpreting this given the changing data quality in the 20CR over time. Nonetheless, we assert that long-term reconstruction is helpful for contextualising recent storminess and for identifying emerging changes in regional hydroclimate linked to cyclones.

Key words: cyclone; storm; 20th Century Reanalysis; North Atlantic storm track; North Atlantic Oscillation; British-Irish Isles precipitation

Corresponding author:

Tom Matthews, School of Natural Sciences and Psychology, Liverpool John Moores University, Liverpool, UK.

E-mail: t.r.matthews@ljmu.ac.uk

1. Introduction

Extra-tropical cyclones are of tremendous physical and societal importance due to their role in redistributing heat, moisture and momentum between latitudes and the extreme surface weather events associated with their passing. The climatological significance of cyclones (or 'storms') is particularly apparent for the British-Irish Isles (BI) as the North Atlantic storm track crosses these densely-populated islands year-round (Woolings, 2010). Producing long-term cyclone climatologies for this region has, therefore, attracted attention from the research community (e.g. Sweeney, 2000; Hickey, 2003, 2011; Hanna et al., 2008; Allan et al., 2009; Cornes and Jones, 2011), not least because this area of the North Atlantic is projected to experience enhanced winter cyclone activity as the climate warms (Woolings et al., 2012; Collins et al., 2013; Feser et al., 2014 and references therein). Long-series of observed cyclonicity provide a means to contextualize apparently 'extreme' seasonal storminess (e.g. Blackburn et al., 2008; Dong et al., 2013a; Matthews et al., 2014) as well as to benchmark emerging trends.

Some long-term cyclone climatologies for Europe and/or the BI have used extreme wind speeds as a proxy for storminess, derived from direct surface observations (e.g. Sweeney, 2000; Hickey 2003, 2011) or geostrophic principles applied to air pressure records (Alexandersson et al., 1998, 2000; Matulla et al., 2008; Wang et al., 2009; Cornes and Jones, 2011). Others have scrutinized high-frequency air pressure variability (Hanna et al., 2008; Allan et al., 2009), or have used tide gauge data (Woodworth and Blackman, 2002; Vilibic and Sepic, 2010; Esteves et al., 2011) to assess historic storminess. Thus, existing work has relied largely upon in-situ measurements from long-running weather/oceanographic stations to serve as a proxy for cyclone frequency and intensity. Feature identification/tracking algorithms which detect cyclones from gridded pressure fields offer scope for identifying and characterising cyclones explicitly. Such techniques have yielded cyclone climatologies of the North Atlantic and beyond (Simmonds and Keay, 2000; Wang et al., 2006; Raible et al., 2008), but have rarely been used to gain insight into the cyclone climatology of the BI in particular. Historically, this is explained by the brevity of reanalysis products (~50 years) compared with station data.

However, the advent of the 20th Century Reanalysis V2 dataset (hereafter 20CR: Compo et al., 2011), permits storm reconstruction back to the 1870s. For example, Wang et al. (2013) used the 20CR to identify cyclones over the extra-tropics in both hemispheres, whilst Jones et

al. (2013) used this dataset to produce an objective catalogue of Lamb Weather Types (LWTs) for the BI. In addition, Wang et al. (2014) presented a 'Cyclone Activity Index' (defined in Section 4), and a time series of extreme wind speeds for the North Sea region. Despite the potential that 20CR offers for providing insights into long-term cyclone characteristics (Cornes, 2014) it has not yet been used to construct a cyclone climatology for the BI. We address this gap and seek to complement and extend long-running storminess metrics provided by station-based methods.

2. Aims and Objectives

Our main aim is to derive a long-term cyclone record for the BI based on 20CR. Our objectives are to 1) establish the seasonal climatology of cyclones over the region, including their influence on precipitation totals; and 2) explore interannual variations in cyclone activity for the study area linked to large-scale atmospheric circulation.

We pursue objective 1 because despite the recognised role of cyclones as an important feature of the BI climate, and of precipitation and flood frequency in particular (Allan et al., 2009; Pattison and Lane, 2012; Wilby and Quinn, 2013), relatively little attention has been directed toward their seasonal characteristics, or influence on surface climate. In constructing the longest direct record of BI cyclonicity to-date, our study is well placed to make a contribution in this regard. Objective 2 is addressed because changes in cyclone activity over the region and their drivers are of the utmost societal concern. Our study allows emergent cyclone properties to be viewed in the context of a 142-year period, facilitating assessment of low-frequency variations in cyclone activity and the role of wider-scale atmospheric processes in driving cyclone activity.

The following sections provide details of the data (Section 3) and methods (Section 4) used in our study, before proceeding to the results in Section 5. There we outline the role of cyclones within the regional hydroclimate (5.1) and interpret the temporal variability in cyclone activity, including coupling to larger-scale atmospheric processes (5.2). These results are then discussed in Section 6 and conclusions are drawn in Section 7.

3. Data

3.1 The Twentieth Century Reanalysis V2

The 20CR project is described in detail by Compo et al. (2011). Briefly, the product provides a comprehensive tropospheric reanalysis spanning the period 1871-2012 at 2° × 2° spatial

resolution, based on a 56-member ensemble using only observations of surface air pressure, sea surface temperatures, and sea ice extent. Uncertainty in the reanalysis is quantified by the spread among ensemble members. Here 20CR data were extracted for each ensemble member at six-hourly resolution (1871-2012: provided by NOAA/OAR/ESRL PSD available at http://www.esrl.noaa.gov/psd/) for the BI domain (50°N to 60°N, 16°W to 6°E) used by Matthews et al. (2014).

Whilst the accuracy of 20CR is described as equivalent to contemporary three-day numerical weather predictions, quality in the earlier part of the record has been questioned in assessments of storminess, particularly for data-sparse periods and regions (Wang et al., 2013; Krueger et al., 2014). In particular, variations in the number of observations assimilated into the 20CR through time challenges the identification of trends in storm activity (Section 4.2), as detected changes may be a spurious consequence of changing data quality (Wang et al., 2013). However, previous research suggests that the 20CR is most likely of good quality and homogeneous throughout the BI region (Wang et al., 2014; Matthews et al., 2014). Figure 1 shows that data quality over the BI and Western Europe is less uncertain and quality degrades relatively little earlier in the record, compared with the mid/high latitude Northern Hemisphere as a whole. Thus, our domain is amongst the most stable regions and, therefore, amenable to producing a robust, long-term cyclone climatology from the 20CR.

3.2. Lamb Weather Types and Precipitation

To corroborate our 20CR cyclone climatology we compared cyclone counts with the number of pure and hybrid cyclonic Lamb Weather types (LWTs) classified objectively by Jones et al. (2013) centred on the BI using the 20CR for the period 1871-1947, and the National Centers for Environmental Prediction/National Centre for Atmospheric Research Reanalysis (NCEP/NCAR: Kalnay et al., 1996) for the period 1948-present. The cyclonic LWTs are a useful comparison for our counts because the former have a long legacy in regional climatology (Lamb, 1972) and the Jones et al. (2013) version of the catalogue employed here has already demonstrated wider utility in hydrological assessment for the BI back to the 19th Century (e.g. Wilby and Quinn, 2013). We refer to pure and hybrid cyclonic LWTs following the terminology of Lamb (1972), whereby hybrids are those which are a mix of pure synoptic (in this case cyclonic) and directional circulations (e.g. northwest). Objective rules for determining the LWTs are based on geostrophic flow strength/direction and relative vorticity; a description of this scheme can be found in Jones et al (1993, 2013).

In exploring seasonal cyclone climatologies we assessed the correlation between cyclone metrics and rainfall totals in the gridded CRU TS3.21 dataset (Harris et al., 2014) which covers the period 1901-2012 at 0.5° × 0.5° spatial resolution. We also use the long-running England and Wales Precipitation (EWP) record (Alexander et al., 2001) to assess any association between years of extreme cyclone activity and precipitation.

To determine links between large-scale atmospheric processes and interannual variability in cyclonicity, we used three indices to describe atmospheric flow in the North Atlantic region: the North Atlantic Oscillation Index (NAOI: Hurrel, 1995), Greenland Blocking Index (GBI: Fang, 2004), and the Blocking Index of Tibaldi and Molteni (1990), extended to two dimensions (Scherrer et al., 2006), and hereafter referred to as BITM. This index identifies blocks by a meridional reversal of the normal poleward geopotential height gradient at the 500 hPa level. The GBI and BITM were thus calculated using the height field of the 500 hPa surface extracted from the 20CR at monthly and daily resolution, respectively. Two versions of the NAOI were used: a principal component (PC) series, derived from the monthly mean 20CR sea-level pressure fields, and the station-based index (data provided by the Climate Analysis Section, NCAR available at: https://climatedataguide.ucar.edu/climate-data/hurrell-north-atlantic-oscillation-nao-index-station-based).

4. Methods

4.1Cyclone Identification and Metrics

Following Matthews et al. (2014) cyclones were identified using an objective algorithm: an implementation of the Serreze et al. (2008) scheme for a regular latitude/longitude grid. The technique classifies cyclones based on the local Laplacian of sea-level pressure. As in Matthews et al. (2014) we apply a threshold criterion that a sea-level pressure gradient of at least 1 hPa 250 km^{-1} must be present between a low centre and surrounding cells to qualify as a cyclone.

The algorithm was applied by scanning each six-hourly grid from the 56 ensemble members separately. When a cyclone is identified, the location (lat/lon) of the cyclone centre and local Laplacian (intensity: L) are stored. Three cyclone metrics for the BI domain were tallied at seasonal resolution: cyclone counts ($C_{i,j}$), which are simply the number of cyclone centres observed in all grids during year i and season j (note that this measure is equivalent to the "cyclone centre count" as defined in Neu et al., 2013); mean cyclone intensity ($\bar{L}_{i,\ j}$)z calculated as the arithmetic mean of the local Laplacians for the $C_{i,j}$ cyclones; and the

Cyclone Activity Index (*CAI*: Wang et al., 2006), given by $CAI_{i,j} = C_{i,j}\bar{L}_{i,j}$. The *CAI* thus weights total counts by mean cyclone intensity. Note that the Laplacian is equivalent to the geostrophic relative vorticity around the cyclone centre and is, therefore, an indicator of low-level convergence. We follow the terminology of Matthews et al. (2014) and refer to the *CAI* as 'storminess' hereafter. Metrics were calculated for each of the 56 ensemble members then averaged to produce an ensemble-mean series. Seasons were defined as successive three-month blocks with winter as December (from previous calendar year) to February.

4.2 Interannual variability in cyclonicity

To assess interannual variability in BI cyclonicity we calculated trends in cyclone metrics over the 142-year (1871-2012) period and examined periods of enhanced storminess cyclone activity in detail. Trends were defined using the non-parametric Theil-Sen slope estimation method (Theil, 1950; Sen, 1968). This metric gives a robust estimate of linear trend in the presence of outliers by using the median slope from an ensemble of trends calculated between every pair of *x*-*y* data coordinates. Trend significance (two-tailed) was assessed using the non-parametric Mann-Kendall test (Mann, 1945; Kendall, 1975). Although we report significance for all statistical tests at the 5% level, these values should be interpreted with caution. There is growing recognition that statistical significance is challenging to establish due to the difficulty of defining a valid null hypothesis in poorly understood physical systems (see Cohn and Lins, 2005), as well as dependency of trend significance on choice of start and end dates (e.g. Murphy et al., 2013).

We also recommend that trends should be viewed critically. Although reanalysis projects employ a physically-consistent and temporally-fixed framework for assimilating data, the spatial density of climate observations is not constant though time, which means that archives cannot be considered homogeneous (Chang and Fu, 2002; Smits et al., 2005; Hanna et al., 2008). This problem is apparent for reanalysis datasets in general, and can result in spurious variability and trends (Dee et al., 2014). Whilst attempts have been made to correct for inhomogeneities in the 20CR itself (Wang et al., 2013), these corrections are not without a degree of subjectivity, as statistically-identified change points used to correct data may reflect legitimate climatic variations. Faced with these complexities we, therefore, select the simplest and most transparent solution of reporting trends based on raw 20CR data and use the significance as a relative indicator of trend strength. The trend analysis is thus included for completeness and comparison with previous studies. Note that the 20CR has been used in the

same unadjusted format for the relatively high-quality data of the BI region by Jones et al. (2013), Donat et al. (2011) and Brönnimann et al., (2012), with the latter two studies also conducting trend analyses on these unadjusted data.

Individual seasons and spells of enhanced cyclone activity were identified by ranking years and decades according to each cyclone metric. Years characterised as extreme were used to explore the role of wider-scale atmospheric processes in driving enhanced cyclone frequency and intensity. This was achieved by compositing standardized 500 hPa height anomalies for those seasons in the top 5% when ranked by the respective cyclone metric (cyclone frequency or intensity). The 500 hPa surface was chosen for analysis as this provides information about atmospheric flow in the mid- and upper-troposphere, permitting insight into the dynamical process generating and steering storms over the North Atlantic.

Linear associations between BI cyclone frequency and intensity with wider-scale circulation were explored by calculating Pearson product-moment correlation coefficients between these variables and the NAOI, GBI and BITM. The NAOI was calculated as the monthly time series of the leading empirical orthogonal function of sea-level pressure over the region 20-80°N, 40-90°W (e.g. Blessing et al., 2005; Hanna et al., 2014), whilst the GBI was computed as the geopotential monthly height anomaly for the 500 hPa surface over the region 60-80°N, 20-80°W (Fang, 2004; Hanna et al., 2013). BITM was calculated for the Atlantic sector (34-76°N, 84°W-44°E) following the method outlined in Scherrer et al. (2006). Unless otherwise stated, all correlations cited below are regarded significant when $p \leq 0.05$.

5. Results

5.1 Cyclone metrics, Lamb Weather Types and rainfall

Correlations between our (20CR) cyclone counts and total pure and hybrid cyclonic LWTs (Figure 2) are all statistically significant. Correlation strength is generally greater between 20CR and hybrid cyclonic weather types and in winter. 20CR total cyclone counts are higher (lower) than the number of pure (hybrid) cyclonic LWTs, consistent with the findings of Matthews et al. (2014) for their winter-only assessment. The overestimation compared to counts of pure cyclonic LWTs may be because we sample the pressure field more frequently (six-hourly here *versus* 24-hourly in the LWT analysis), meaning that short-lived lows are more likely to be detected. The fact that the number of hybrid cyclonic LWTs exceeds our cyclone counts could be due to the more stringent definition of a cyclone employed here,

which includes an intensity threshold. This may also explain why correlation between LWT counts and our cyclone metrics are weaker outside of winter. Mean cyclone intensity is lower in warmer months and, in the presence of weaker lows, there is evidently a greater chance of disagreement in the detection of a cyclone according to these classification schemes (see below for details of the seasonal cycle in cyclone intensity).

Correlation surfaces for interannual seasonal rainfall variability and cyclone metrics are shown in Figure 3. Correlations between our metrics and rainfall are significant not just for the BI, but for large parts of northwest Europe. Maps of counts and storminess appear similar because interannual variations in storminess are mainly driven by cyclone counts. This metric has a higher standard deviation than intensity when expressed as a percentage of the mean (C_v of 18.7% *versus* 6.0%: see Table 1 and Section 5.3) and storminess is calculated with a multiplicative formula (Section 4.1). For conciseness, we focus on the correlation for cyclone counts.

In winter, an area of significant positive correlations with cyclone frequency extends over much of northwest Europe, with the exception of western Scandinavia which registers significant negative correlations. In summer, the area exhibiting significant correlations between the cyclone metrics and precipitation contracts and the strength of the correlations throughout northern Europe is also generally lower, particularly for western Scandinavia. However, average correlation strength is greatest across the BI during summer and there is a weak spatial gradient in correlation across the domain. This is unlike winter where there is a noteworthy decrease in the strength of the correlation between cyclone count and precipitation with increasing latitude, becoming non-significant for northwest Scotland. In this region, cyclone intensity is significantly correlated with precipitation.

The seasonal regime of cyclone metrics is illustrated in Figure 4. Mean cyclone intensity progresses from a maximum during winter to minimum in summer. The seasonal change in counts is more complex. The probability of cyclone presence over the BI is greatest in late summer (August), with secondary peaks in late spring (May) and late autumn (November). Minimum cyclone frequency occurs in winter. Further insight into this aspect of cyclonicity of the region is provided by Figure 5, where counts are aggregated into three-month seasons for consecutive 30-year periods (except the abridged period 1991-2012). The summer peak in cyclone frequency is evident again, but interestingly the seasonal maxima is absent from 1961-1990. According to Figure 4, the stormiest period for the BI generally occurs in late

autumn, as the secondary peak in cyclone frequency combines with the symmetrical cycle in intensity which ascends from the summer minima.

5.3 Interannual variability in BI cyclonicity

Annual and seasonal series of cyclone metrics are shown in Figure 6; coefficients of variation and linear trends are presented in Table 1. Cyclone counts exhibit greatest year-to-year variability. Seasonally, both cyclone frequency and intensity are most variable in winter, with the standard deviation exceeding 40% of the mean for the former. Regarding trends, counts in all seasons have decreased over the period analysed, but the decline is weak and non-statistically significant. Stronger trends are observed for mean cyclone intensity which has increased in all seasons, with the strongest and weakest trends in winter and summer, respectively. The counteracting effects of decreasing cyclone counts with increased mean intensity, results in no net change in storminess throughout the period of study: trends for this metric are increasing for all seasons except spring, but all are very weak and statistically insignificant.

The top seven years (corresponding to ~5% of the record) by cyclone frequency, intensity and storminess are shown in Table 2, while inter-decadal variation in cyclonicity is ranked and illustrated in Figure 7. The stormiest year was 1872 due to high cyclone frequency in winter and autumn. More recently, the years 2000 and 2009 feature as extreme and summer 2012 also registers as exceptional. This extreme seasonal storminess joins the winter of 2013/2014, which Matthews et al. (2014) determined as unprecedented since 1871/72 by updating the winter 20CR BI cyclone series to 2013/2014 using the NCEP reanalysis. The stormiest decade was the 1910s, mainly due to frequent cyclones in winter and spring. The second and third stormiest decades were the 1920s and 1980s respectively, with the 1920s peak driven by frequent cyclones in spring, summer and autumn, which were also intense in the latter two seasons. The storminess of the 1980s is due to very high cyclone intensity: this decade experienced the most intense cyclones in every season except winter, where it ranked second according to this metric. The quietest decade for storminess was the 1970s on account of the relatively low number of cyclones in spring and summer. The decades of lowest cyclone intensity are mainly found in the earlier part of the record in all seasons, with the 1870s, 1880s and 1890s ranked 14th, 13th and 12th, respectively. This is consistent with the strongly increasing trends found for this metric (Table 1).

5.4 BI cyclonicity and atmospheric circulation

To explore how the frequency and intensity of cyclones relate to larger-scale atmospheric circulation, we used the years listed in Table 2 to produce composite plots of anomalies at the 500 hPa level (Figure 8). The most coherent anomalies are observed for winter when high cyclone frequency is associated with a low height anomaly over a broad region of the northeast Atlantic, approximately centred over the BI. The downstream anomaly is reminiscent of a Rossby wave train with alternating high/low height anomalies, whilst upstream there is a suggestion of higher geopotential heights in the vicinity of Greenland. A clear geopotential height anomaly signal also emerges in winter when cyclone intensity is considered. Seasons with more intense cyclones are characterised by a height field with positive (negative) anomalies in the low (high) latitudes of the North Atlantic. Outside of winter, coherence in the anomaly field for years of extreme cyclonicity is less evident for both cyclone counts and intensity. In all seasons more frequent cyclones act to lower geopotential heights in the vicinity of the BI.

To further investigate the link between cyclonicity and larger scale atmospheric circulation we also determined associations between cyclone metrics and indices of atmospheric circulation in the North Atlantic region. As the BITM is a two-dimensional index, we explore associations between blocking frequency at each grid point and cyclone frequency/intensity (Figure 9). For all seasons an increase in cyclone frequency for the BI is associated with a decrease in blocking over the region and an increase in blocking at higher latitudes over the Atlantic. In winter the area of significant positive correlations between high-latitude blocking and BI cyclone frequency is relatively extensive, with significant correlations found to the west and east of Greenland. In other seasons, positive correlations only persist to the east. In spring, summer, and autumn, cyclone intensity generally exhibits weaker correlations (than frequency) with blocking. During the winter months, cyclones over the BI tend to be more intense when blocking is increased (decreased) to the south (north) of the islands.

Correlations between the cyclone metrics and the NAOI and GBI are provided in Table 3. For comparison, and on the basis of Figure 9, we also report correlations between blocking frequency for the BI domain (50-60°N, 16°W-6°E; hereafter ‘BIBF’ - BI Blocking Frequency) and cyclone frequency/intensity. BIBF is defined as the daily probability of at least one grid cell being blocked within the BI domain. The strongest correlations for cyclone counts are observed for BIBF, but significant correlations are similarly apparent between frequency and both the NAOI and GBI. These indices are also significantly correlated with average cyclone intensity. The results indicate that periods of positive (negative) NAO (GBI) conditions are

associated with fewer, but more intense cyclones over the BI. This relationship breaks down somewhat in summer (no significant correlation with cyclone intensity) and autumn (no significant correlation with cyclone frequency), but is otherwise persistent. This is characteristic of the fact that, with the exception of the association between BIBF and counts, correlations between cyclone metrics and circulation indices are generally strongest in the winter.

6. Discussion

6.1 BI cyclonicity and regional hydroclimate

The 142-year record yields new insights into the cyclone climate of the BI. Strong and statistically significant correlations between seasonal precipitation and cyclone frequency confirm the regional hydroclimatic importance of cyclones. The stormiest periods have also been recognised as extreme in other hydroclimatic indicators: e.g. the top-ranking winter (1915) and autumn (2000) are the wettest in the long-running EWP series for the overlapping period (1871/72-2012), whilst the stormiest spring (1983) and summer (2012) also rank highly (4^{th} and 3^{rd}, respectively). Extensive seasonal flooding has additionally been documented during periods recognized as extremely stormy: e.g. autumn 2000 (Marsh and Dale, 2002; Jones et al., 2006), and summer 2012 (Parry et al., 2012; Dong et al., 2013a). Moreover, the stormiest year (1872) is wettest in the EWP series and has been noted as a particularly flood-rich period (Jones et al., 2006; Wilby and Quinn, 2013). The most subdued decade in terms of storminess (the 1970s) was a period of exceptional drought in the BI (Jones et al., 2006; Marsh et al., 2007; Rodda and Marsh, 2011; Murphy et al., 2013). Correspondence with independent hydroclimatic indicators highlights the importance of cyclones for the regional hydroclimate, and simultaneously corroborates the 20CR cyclone reconstruction.

Correlation between precipitation and cyclone counts was highest during summer. This differs from Lavers et al. (2013), who found the relationship between mean sea-level pressure (MSLP) and precipitation across northwest Europe (including the BI) was weaker in summer than in winter. One explanation for this discrepancy is that the storm track is known to be more spatially restricted in summer than winter over the northeast Atlantic (Mesquita et al. 2008). Thus, where cyclone frequency is an important driver of precipitation totals, it is reasonable to expect that regions of significant correlations between rainfall totals and MSLP (which bare the imprint of depression passage) should be similarly constrained. The different

period (1957-2002) and spatial resolution (2.5° × 2.5°) of the reanalysis dataset used by Lavers et al. (2013) could be another factor. In highlighting the importance of cyclones in driving high precipitation amounts over the BI throughout the year, our results agree with Murphy and Washington (2001), who, in all seasons, observed a cyclonic pattern in the correlation field centred on the BI when assessing the association between mean sea-level pressure and the leading Empirical Orthogonal Function of BI rainfall.

Correlations between summer precipitation and summer cyclone counts are more spatially-consistent over BI relative to other seasons. During winter, correlations between cyclone counts/storminess, and precipitation are insignificant for the northwest of our domain where we observed stronger correlations between cyclone intensity and precipitation. Periods of enhanced cyclone intensity for the BI have been associated with positive phases of the NAO (Allan et al., 2009, and see Section 6.2). This correspondence is strongly hinted at in Figure 3 as the correlation between BI cyclone intensity and precipitation mirrors the association between the NAOI and European winter precipitation (Wilby et al., 1997; Trigo et al., 2002), reflecting the more northerly (southerly) position of the storm track during NAO positive (negative) conditions. When cyclones take a more northerly route over the northeast Atlantic, they will not be counted in our BI domain but may still enhance seasonal precipitation in the northwest BI through the passage of trailing fronts. During positive NAO conditions, the stronger westerly flow is also understood to increase orographic rainfall for the British uplands (Burt and Holden, 2013). These mechanisms explain the lack of correlation between cyclone counts and precipitation in the northwest in winter: precipitation can be enhanced in the northwest BI by the passage of "local" cyclones (which will register in our counts) through low-level convergence and frontal lifting, but also by "remote" cyclones north of our domain, as both trailing fronts and enhanced orographic uplift associated with a more northerly storm track are important rainfall generating mechanisms. We suggest that in winter the latter are more important, due to the stronger westerly flow, but that in summer the former emerges as dominant when the westerly flow weakens (cf. Wilby et al., 2002). This would also account for the more spatially homogenous summer correlation field in Figure 3. Regardless of the physical processes driving correlations, cyclone frequency has already been linked to spatially-extensive flooding episodes (Wilby and Quinn, 2013) due to high rainfall amounts across the BI associated with cyclone passage (Burt et al., 2014). We emphasise that these conclusions are perhaps *most* appropriate for summer based on the evidence presented here.

6.2 Atmospheric circulation and temporal variability in BI cyclonicity

Days with cyclonic circulation over the BI are most frequent in summer. This finding is consistent with Mesquita et al. (2008) who showed that the northeast North Atlantic is among the few regions in the Northern Hemisphere to experience a summer cyclone maximum. The assessment of cyclonicity (Section 5.4) provides some insight to physical processes driving the seasonal cycle in cyclone frequency. Cyclone counts were found to correlate most strongly with the BIBF, such that increased regional blocking translates into fewer cyclonic circulation days. This fits with the summer-only investigation of Dong et al. (2013b) and agrees with the negative correlation between cyclonic and anticyclonic LWTs noted by Burt et al. (2014). Figure 10 (left) demonstrates that this relationship generally holds when the seasonal climatological cycle is assessed: the blocking minimum in summer, characteristic of conditions across the north-eastern margin of Europe (Figure 10 - right), coincides with the summer cyclone maxima. The relationship between interannual blocking and cyclone frequency is further highlighted by anomalous conditions during the 1961-1990 climate normal period (cf. Section 6.1and Figure 5), during which the summer cyclone maximum was not observed. This was also a 30-year period characterised by frequent summer blocking (Table 4). It is interesting to note that a 30-year period (1961-1990) widely used to define climate normals was actually highly unusual from the perspective of summer atmospheric circulation for the BI.

To assess the role of larger-scale atmospheric processes modulating BI cyclonicity climate, we correlated cyclone metrics with climate indices. The GBI and NAOI exhibited correlation coefficients that were opposite in sign, which is unsurprising given the association between Greenland blocking and the NAO (Woolings et al., 2008). As correlations were stronger for the NAOI, we focus on this index here. Interannual variability in cyclone frequency was generally found to be negatively correlated with the NAOI in most seasons, the signal being strongest (highest *r* values) using the PC-based NAOI, and in winter. The sign of relationship is consistent with analyses using the cyclonic LWT (e.g. Wilby et al., 1997; Burt et al., 2014). Negative correlation may reflect either slower-moving cyclonic systems during NAO negative years (subdued westerly circulation), or the passage of more cyclonic weather systems, as both processes could contribute to a higher number of cyclone days for our domain.

Cyclone intensity was positively correlated with the NAOI in most seasons, with strongest associations in winter, which concurs with Allan et al. (2009) and Wang et al. (2009, 2011). The relationship between the NAO and cold-season cyclone intensity is also consistent with the intense winter storminess identified during the 1990s (exceptionally positive NAO - see Hanna et al., 2014)) in this study (Section 5.4) and in previous investigations (Jones et al., 1999; Allan et al., 2009; Wang et al., 2009, 2011; Cornes and Jones, 2011; Donat et al., 2011). Whilst the NAOI exhibits statistically significant correlations with our cyclone metrics, we note that even during winter when these associations are strongest, the NAO only accounts for ~16 and 31% of the variance in cyclone frequency and intensity, respectively. Thus, the utility of the NAO for interpreting BI cyclonicity is perhaps limited (cf. Burningham and French, 2013).

Our results suggest an increase in cyclone intensity for all seasons over the BI that is strongest in winter. Detailed comparison with other research is confounded by differences in the choice of metrics, domains and sampling resolutions. However, increased BI cyclone intensity is broadly supported by investigations of trends in extreme wind speeds using the 20CR (Brönnimann et al., 2012; Donat et al., 2012) and by Wang et al. (2013) who found increasing mean Laplacian from the 20CR for the high-latitude North Atlantic (in which our domain is mostly situated). These results stand in contrast with studies using in-situ pressure observations to determine changes in BI cyclone intensity (e.g. Hanna et al., 2008; Wang et al., 2009, 2011). Although such contradictions regarding the 20CR has been raised before (Krueger et al., 2014; Wang et al., 2014) the cause remains unclear. Improved understanding of this disagreement is needed as enhanced cold-season cyclone intensity has been projected for the BI region (Collins et al., 2013; Zappa et al. 2013; Feser et al., 2014). Robust long-term cyclone climatologies are required if emerging trends are to be differentiated from natural variability.

Cyclone frequency and storminess were more closely related to interannual variation in BI precipitation. Recent years have seen three of the stormiest seasons on record, with autumn (2000) and summer (2012) joining the winter of 2013/2014 (see Matthews et al. (2014)) as the most exceptional seasons since the beginning of 20CR. Despite this clustering, we detected no evidence for an upward trend in storminess, reflecting the signal (or lack of) in cyclone frequency compared to the noise of interannual variability. However, pronounced, low-frequency variability in these metrics is evident, which underscores the utility of the long-term cyclone climatology presented here in contextualising recent extremes. For

example, the highly-subdued storminess observed during the 1961-1990 climate normal period has perhaps made the return to more typical conditions in recent years seem unusual. Trends with start dates during this quiescent period are likely to be misleading: calculating the Mann Kendall test statistic on the period 1979-2012 (the period of satellite observation that signals the start date of the ERA-Interim Reanalysis dataset: Dee et al. (2011)), yields upward trends in summer cyclone frequency and storminess with *p*-values of 0.017 and 0.044, respectively. Thus, despite the higher quality of more recent gridded data products for objective assessment of atmospheric circulation, there remains a need for the longer-term perspective afforded by products such as the 20CR is clear.

7. Conclusions

We have constructed a 142-year cyclone climatology for the BI using the 20CR. This product both confirms and clarifies the importance of cyclones to the hydroclimate of this region. Seasonal precipitation totals were found to be strongly correlated with cyclone frequency across large parts of the BI, but this is most apparent during the summer, when these weather types are more frequent. We therefore conclude that any changes in the frequency of "local" cyclones for the region would be particularly important for seasonal precipitation totals during summer. In this context, we detected no trend in cyclone frequency or storminess in any season, but did establish that the 1961-1990 climate normal was extraordinary for the rarity of summer cyclones, which is consistent with the severe droughts reported for the same period. Such low-frequency variability in cyclone frequency was found to be strongly associated with atmospheric blocking – a control which also emerged when the seasonal cycle in this metric was assessed. Thus, we emphasise that to better understand the processes driving variability in the frequency of cyclones for the BI, it is necessary to investigate mechanisms that modulate atmospheric blocking in the Euro-Atlantic sector.

Cyclone intensity was observed to be significantly correlated (positive) with the NAOI, particularly in winter, which is generally in agreement with the literature. However, our detection of a strong upward trend in cyclone intensity highlights a discrepancy between long-term reanalysis reconstructions and assessments of cyclone intensity based on station data. Given expectations of enhanced cyclone activity for the BI in a warmer climate, we emphasise that resolving this matter should be a high priority for future research.

References

Alexander LV and Jones PD. 2001. Updated precipitation series for the UK and discussion of recent extremes. *Atmos. Sci. Let.* **1**: 142-150.

Alexandersson H. Schmith T, Iden K. and Tuomenvirta H. 1998. Long-term variations of the storm climate over NW Europe. *The Global Atmosphere and Ocean System* **6**: 97-120.

Alexandersson H, Tuomenvirta H, Schmith T and Iden K. 2000. Trends of storms in NW Europe derived from an updated pressure data set. *Clim. Res.* **14**: 71-73.

Allan R, Tett S and Alexander L. 2009. Fluctuations in autumn–winter severe storms over the British Isles: 1920 to present. *Int. J. Climatol*. **29**: 357–371.

Blackburn M, Methven J and Roberts N. 2008. Large-scale context for the UK floods in summer 2007. *Weather* **63**: 280-288.

Blessing S, Fraedrich K, Junge M, Kunz T, Lunkeit F. 2005. Daily North-Atlantic Oscillation (NAO) index: Statistics and its stratospheric polar vortex dependence. *Meteorol. Z.* **14**: 763–769.

Brönnimann S, Martius O, Von Waldow H, Welker C, Luterbacher J, Compo GP, Sardeshmukh PD, and Usbeck T. 2012. Extreme winds at northern mid-latitudes since 1871. *Meteorol. Z.* **21**: 13-27.

Burningham H and French J. 2013. Is the NAO winter index a reliable proxy for wind climate and storminess in northwest Europe?. *Int. J. Climatol*., **33**: 2036-2049.

Burt TP and Howden NJK. 2013. North Atlantic Oscillation amplifies orographic precipitation and river flow in upland Britain. *Water Resour. Res*. **49**: 3504–3515.

Burt TP, Jones PD and Howden NJK. 2014. An analysis of rainfall across the British Isles in the 1870s. *Int. J. Climatol*. DOI: 10.1002/joc.4184

Chang EKM and Fu Y. 2002. Interdecadal variations in Northern Hemisphere winter storm track intensity. *J. Climate* **15:** 642–658.

Cohn TA and Lins HF. 2005. Nature's style: Naturally trendy. *Geophys. Res. Lett* **32**: L23402.

Collins M, Knutti R Arblaster J Dufresne J-L, Fichefet T, Friedlingstein P, Gao X, Gutowski WJ, Johns T, Krinner G, Shongwe M, Tebaldi C, Weaver AJ and Wehner M. 2013: Long-term Climate Change: Projections, Commitments and Irreversibility. In: Climate Change 2013: The Physical Science Basis. Contribution of Working Group I to the Fifth Assessment Report of the Intergovernmental Panel on Climate Change [Stocker TF, Qin D, Plattner G-K, Tignor M, Allen SK, Boschung J, Nauels A, Xia Y, Bex V and Midgley PM (eds.)]. Cambridge University Press, Cambridge, United Kingdom and New York, NY, USA.

Compo G P, Whitaker JS, Sardeshmukh P D, Matsui N, Allan RJ. Yin X, Gleason BE, Vose RS, Rutledge G, Bessemoulin P, Brönnimann S. Brunet M, Crouthamel RI, Grant AN, Groisman PY, Jones PD, Kruk MC, Kruger AC, Marshall GJ, Maugeri M, Mok HY, Nordli Ø, Ross TF, Trigo RM, Wang XL, Woodruff SD and Worley SJ. 2011. The Twentieth Century Reanalysis Project. *Q.J.R. Meteorol. Soc*. **137**: 1–28.

Cornes RC and Jones PD. 2011. An examination of storm activity in the northeast Atlantic region over the 1851–2003 period using the EMULATE gridded MSLP data series. *J. Geophys. Res*. **116**: D16110.

Cornes RC. 2014. Historic storms of the northeast Atlantic since circa 1700: a brief review of recent research. *Weather* **69**: 121–125.

Dee DP, Uppala SM, Simmons AJ, Berrisford P, Poli P, Kobayashi S, Andrae U, Balmaseda MA, Balsamo G, Bauer P, Bechtold P, Beljaars ACM, Van de Berg L, Bidlot J, Bormann N, Delsol C, Dragani R, Fuentes M, Geer AJ, Haimberger L, Healy SB, Hersbach H, Hólm EV, Isaksen L, Kållberg P, Köhler M, Matricardi M, Mcnally AP, Monge-sanz BM, Morcrette J, Park B, Peubey C, de Rosnay P, Tavolato C, Thépaut J and Vitart F. 2011. The ERA-Interim reanalysis: configuration and performance of the data assimilation system. *Q.J.R. Meteorol. Soc* **137**: 553-597.

Dee D, Fasullo J, Shea D, Walsh John and National Center for Atmospheric Research Staff (Eds). *The Climate Data Guide: Atmospheric Reanalysis: Overview & Comparison Tables*. Retrieved from https://climatedataguide.ucar.edu/climate-data/atmospheric-reanalysis-overview-comparison-tables. Last modified 05 Nov 2014.

Donat MG, Renggli D, Wild S, Alexander LV, Leckebusch GC, Ulbrich U. 2011. Reanalysis suggests long-term upward trends in European storminess since 1871. *Geophys. Res. Lett.* **38**: L14703.

Dong B, Sutton R and Woolings T. 2013a. The extreme European Summer 2012 [in "Explaining Extreme Events of 2012 from a Climate Perspective]. *Bull. Amer. Meteor. Soc* **9**: s28-s32.

Dong B, Sutton RT, Woollings T and Hodges K. 2013b. Variability of the North Atlantic summer storm track: mechanisms and impacts on European climate. *Environ. Res. Lett.* **8:** 034037.

Esteves LS, Williams JJ and Brown JM. 2011. Looking for evidence of climate change impacts in the eastern Irish Sea. *Nat. Hazard. Earth Sys.* **11**: 1641-1656.

Fang ZF. 2004. Statistical relationship between the northern hemisphere sea ice and atmospheric circulation during wintertime. In *Observation, Theory and Modeling of Atmospheric Variability. World Scientific Series on Meteorology of East Asia*, Zhu X (ed). World Scientific Publishing Company: Singapore; 131–141

Feser F, Barcikowska M, Krueger O, Schenk F, Weisse R and Xia L. 2014. Storminess over the North Atlantic and northwestern Europe—A review. *Q. J. Roy. Meteor. Soc*. DOI: 10.1002/qj.2364

Hanna E, Cappelen J, Allan R, Jónsson T, Le Blancq F, Lillington T and Hickey K. 2008. New insights into North European and North Atlantic surface pressure variability, storminess, and related climatic change since 1830. *Int. J. Climatol.* **21**: 6739-6766.

Hanna E, Jones JM, Cappelen J, Mernild SH, Wood L, Steffen K and Huybrechts P. 2013. The influence of North Atlantic atmospheric and oceanic forcing effects on 1900–2010 Greenland summer climate and ice melt/runoff. *Int. J. Climatol*. **33**: 862–880.

Hanna E, Cropper TE, Jones PD, Scaife AA and Allan R. 2014, Recent seasonal asymmetric changes in the NAO (a marked summer decline and increased winter variability) and associated changes in the AO and Greenland Blocking Index. *Int. J. Climatol*. DOI: 10.1002/joc.4157

Harris I, Jones PD, Osborn TJ and Lister DH. 2014. Updated high-resolution grids of monthly climatic observations – the CRU TS3.10 Dataset. *Int. J. Climatol*. **34**: 623–642.

Hickey KR. 2003. The Storminess Record from Armagh Observatory 1796-1999. *Weather* **58**: 28-35.

Hickey KR. 2011. The hourly gale record from Valentia Observatory, SW Ireland 1874-2008 and some observations on extreme wave heights in the NE Atlantic, *Climatic Change* **106**: 483-506.

Hurrell J W. 1995. Decadal trends in the North Atlantic Oscillation: regional temperatures and precipitation. *Science* **269**: 676-679.

Jones, P. D., Hulme, M., & Briffa, K. R. 1993. A comparison of Lamb circulation types with an objective classification scheme. *Int. J. Climatol*. **13**: 655-663.

Jones PD, Horton EB, Folland CK, Hulme M, Parker DE and Basnett TA. 1999. The use of indices to identify changes in climatic extremes. *Climatic Change* **42**: 131-149.

Jones PD, Lister DH, Wilby RL and Kostopoulou E. 2006. Extended river flow reconstructions for England and Wales, 1865-2002. *Int. J. Climatol*, **26**: 219–231.

Jones PD, Harpham C and Briffa KR. 2013. Lamb weather types derived from reanalysis products. *Int. J. Climatol*, **33**: 1129–1139.

Kalnay E, Kanamitsu M, Kistler R, Collins W, Deaven D, Gandin L, Iredell M, Saha S, White G, Woollen J, Zhu Y, Leetmaa A, Reynolds R, Chelliah M, Ebisuzaki W, Higgins W, Janowiak J, Mo KC, Ropelewski C, Wang J, Jenne R and Joseph D. 1996: The NCEP/NCAR 40-year reanalysis project. *Bull. Amer. Meteor. Soc.* **77**: 437–471.

Kendall MG. 1975. *Rank correlation methods*. Charles Griffin: London

Krueger O, Feser F, Bärring L, Kaas E, Schmith T, Tuomenvirta H and von Storch H. 2014. Comment on Trends and low frequency variability of extra-tropical cyclone activity in the ensemble of twentieth century reanalysis by Xiaolan L. Wang, Y. Feng, GP Compo, VR Swail, FW Zwiers, RJ Allan, and PD Sardeshmukh, Climate Dynamics, 2012. *Clim. Dynam*. **42**:1127-1128.

585 Lavers D, Prudhomme C and Hannah DM. 2013. European precipitation connections with
586 large-scale mean sea-level pressure (MSLP) fields. *Hydrolog. Sci. J* **58**: 310-327.

587 Lamb HH. 1972. British Isles weather types and a register of daily sequence of circulation
588 patterns, 1861-1971: Geophysical Memoir **116** HMSO, London.

589 Mann HB. 1945. Nonparametric tests against trend. *Econometrica* **13**: 245–259.

590 Marsh TJ and Dale M. 2002. The UK Floods of 2000–2001: A Hydrometeorological
591 Appraisal. *Water Environ*. J. **16**: 180–188.

592 Marsh T, Cole G and Wilby RL. 2007. Major droughts in England and Wales, 1800-2006.
593 *Weather*, **62**: 87–93.

594 Matthews T, Murphy C, Wilby RL and Harrigan S. 2014. Stormiest winter on record for
595 Ireland and UK. *Nature Clim. Change* **4**: 738-740.

596 Matulla C, Schöner W, Alexandersson H, Von Storch H and Wang XL. 2008. European
597 storminess: late nineteenth century to present. *Clim. Dynam.* **31**: 125-130.

598 Mesquita MDS, Gunnar Kvamstø N, Sorteberg A and Atkinson DE. 2008. Climatological
599 properties of summertime extra-tropical storm tracks in the Northern Hemisphere. *Tellus A*,
600 **60**: 557–569.

601 Murphy C, Harrigan S, Hall J and Wilby RL. 2013. Climate-driven trends in mean and high
602 flows from a network of reference stations in Ireland. *Hydrolog. Sci. J.* **58**: 755-772.

603 Murphy SJ and Washington R. 2001. United Kingdom and Ireland precipitation variability
604 and the North Atlantic sea-level pressure field. *Int. J. Climatol*. **21**: 939–959.

605 Neu U, Akperov MG, Bellenbaum N, Benestad R, Blender R, Caballero R, Cocozza A, Dacre
606 HF, Feng Y, Fraedrich K, Grieger J, Gulev S, Hanley J, Hewson T, Inatsu M, Keay K, Kew
607 SF, Kindem I, Leckebusch GC, Liberato MLR, Lionello P, Mokhov II, Pinto JG, Raible CC,
608 Reale M, Rudeva I, Schuster M, Simmonds I, Sinclair M, Sprenger M, Tilinina ND, Trigo IF,
609 Ulbrich S, Ulbrich U, Wang XL, and Wernli H. 2013. Imilast: a community effort to
610 intercompare extratropical cyclone detection and tracking algorithms. *Bull. Amer. Meteor.*
611 *Soc.* **94**: 529–547.

612 Parry S, Marsh T and Kendon M. 2013. 2012: from drought to floods in England and Wales.
613 *Weather* **68**: 268–274.

614 Pattison I and Lane SN. 2012. The relationship between Lamb weather types and long-term
615 changes in flood frequency, River Eden, UK. *Int. J. Climatol.* **32**: 1971-1989.

616 Raible CC, Della-Marta PM, Schwierz C, Wernli H and Blender R. 2008. Northern
617 Hemisphere extratropical cyclones: A comparison of detection and tracking methods and
618 different reanalyses. *Mon. Weather Rev.* **136**: 880-897.

619 Rodda JC and Marsh TJ. 2011. The 1975-76 Drought - a contemporary and retrospective
620 review. *National Hydrological Monitoring Programme series*. NERC/Centre for Ecology and
621 Hydrology: Wallingford, UK.

622 Scherrer SC, Croci-Maspoli M, Schwierz C and Appenzeller C. 2006. Two-dimensional
623 indices of atmospheric blocking and their statistical relationship with winter climate patterns
624 in the Euro-Atlantic region. *Int. J. Climatol*. **26**: 233–249.

625 Sen P K. 1968. Estimates of the regression coefficient based on Kendall's tau. *J. Am. Stat.*
626 *Assoc*. **63**: 1379–1389

627 Serreze MC and Barrett AP. 2008. The summer cyclone maximum over the central Arctic
628 Ocean. *J. Climatol*. **21**: 1048-1065.

629 Simmonds I and Keay K. 2000. Mean Southern Hemisphere extratropical cyclone behavior in
630 the 40-year NCEP-NCAR reanalysis. *J. Climatol.* **13**: 873-885.

631 Smits A, Klein Tank AMG and Können GP. 2005. Trends in storminess over the Netherlands,
632 1962–2002. *Int. J. Climatol.* **25**: 1331–1344.

633 Sweeney J. 2000. A three-century storm climatology for Dublin 1715–2000. *Irish*
634 *Geography* **33**: 1-14.

635 Theil H. 1950. A Rank-invariant Method of Linear and Polynomial Regression Analysis I.
636 *Nederlands Akad. Wetensch. Proc*. **53**: 386–392.

637 Tibaldi S and Molteni F. 1990: On the operational predictability of blocking.
638 *Tellus* **42A**:343-365.

639 Trigo RM, Osborn TJ and Corte-Real JM. 2002. The North Atlantic Oscillation influence on
640 Europe: climate impacts and associated physical mechanisms. *Clim. Res.* **20**: 9-17.

641 Vilibić I and Šepić J. 2010. Long-term variability and trends of sea-level storminess and
642 extremes in European Seas. *Global and Planet. Change* **71**: 1-12.

643 Wang XL, Swail VR and Zwiers FW. 2006. Climatology and changes of extratropical
644 cyclone activity: Comparison of ERA-40 with NCEP-NCAR reanalysis for 1958-2001. *J*
645 *Climatol* **19**: 3145-3166.

646 Wang XL, Zwiers FW, Swail VR and Feng Y. 2009. Trends and variability of storminess in
647 the Northeast Atlantic region, 1874–2007. *Clim. Dynam.* **33**: 1179-1195.

648 Wang XL, Wan H, Zwiers FW, Swail VR, Compo GP, Allan, Vose RS, Jourdain S and Yin
649 X. 2011. Trends and low-frequency variability of storminess over western Europe, 1878–
650 2007. *Clim. Dynam.* **37**: 2355-2371.

651 Wang XL, Feng Y, Compo GP, Swail VR, Zwiers FW, Allan RJ and Sardeshmukh PD. 2013.
652 Trends and low frequency variability of extra-tropical cyclone activity in the ensemble of
653 twentieth century reanalysis. *Clim. Dynam.* **40**: 2775-2800.

654 Wang XL. Feng Y, Compo GP, Zwiers FW, Allan RJ, Swail VR and Sardeshmukh PD. 2014.
655 Is the storminess in the Twentieth Century Reanalysis really inconsistent with observations?
656 A reply to the comment by Krueger et al. (2013b). *Clim. Dynam* **42**:1113-1125.

657 Wilby RL, O'Hare G. and Barnsley N. 1997. The North Atlantic Oscillation and British Isles
658 climate variability, 1865–1996. *Weather* **52**: 266–276.

659 Wilby RL, Conway D and Jones PD. 2002. Prospects for downscaling seasonal precipitation
660 variability using conditioned weather generator parameters. *Hydrol. Process.* **16**: 1215–1234.

661 Wilby RL and Quinn NW. 2013. Reconstructing multi-decadal variations in fluvial flood risk
662 using atmospheric circulation patterns. *J. Hydrol.* **487**: 109-121.

663 Woodworth PL and Blackman DL. 2002. Changes in extreme high waters at Liverpool since
664 1768. *Int. J. Climatol*. **22**: 697–714.

665 Woollings T, Hoskins B, Blackburn M and Berrisford P. 2008: A new Rossby wave-breaking
666 interpretation of the North Atlantic Oscillation. *J. Atmos. Sci*. **65**: 609–626.

667 Woollings T. 2010. Dynamical influences on European climate: an uncertain future. *Phios.T*
668 *Roy. Soc. A* **368**: 3733-3756.

669 Woollings T, Gregory J M, Pinto JG, Reyers M and Brayshaw DJ. 2012. Response of the
670 North Atlantic storm track to climate change shaped by ocean-atmosphere coupling. *Nat.*
671 *Geosci*.**5**: 313-317.

672 Zappa G, Shaffrey LC, Hodges KI, Sansom PG and Stephenson DB. 2013: A Multimodel
673 Assessment of Future Projections of North Atlantic and European Extratropical Cyclones in
674 the CMIP5 Climate Models. *J. Climate* **26**: 5846–5862, doi:10.1175/JCLI-D-12-00573.1.

Tables

Table 1. Changes in cyclone metrics time series. Trends (β) are given as change per decade in % of the mean over the whole period. Trend significance (in brackets as a percentage) for the corresponding Mann-Kendall statistic (not shown). Coefficients of variation (C_v: mean/standard deviation) are expressed as a percentage.

	Count (*C*)		**Intensity ($\bar{L}$)**		**Storminess (*CAI*)**	
	β	C_v	β	C_v	β	C_v
DJF	-0.25 (26.8)	41.7	1.23 (100.0)	13.1	0.67 (55.4)	40.8
MAM	-0.86 (74.7)	33.2	0.67 (99.4)	10.5	-0.19 (22.8)	36.5
JJA	-0.41 (42.4)	33.1	0.42 (92.6)	10.3	0.07 (18.4)	36.5
SON	-0.36 (38.0)	36.6	0.83 (99.9)	11.1	0.35 (34.0)	38.2
Full year	-0.51 (79.8)	18.7	0.75 (100.0)	6.0	0.27 (47.4)	18.9

Table 2. Top seven ranked years (i.e. ~5% of the dataset) for each cyclone metric by season. Note that Matthews et al. (2014) found that winter of 2013/14 was the stormiest since 1871/72, based on NCEP reanalysis for years outside the 1871/72-2012 period of 20CR.

Rank	**1**	**2**	**3**	**4**	**5**	**6**	**7**
				Counts			
DJF	1915	1936	1960	1919	1951	1872	1977
MAM	1983	1981	1920	1909	1979	1888	1882
JJA	1927	1879	2012	1888	1912	1917	1882
SON	2000	1872	1935	1976	1960	1896	1974
Full year	1872	1927	1882	1916	1951	2000	1930
				Intensity			
DJF	2012	1989	1990	1995	1993	1952	2000
MAM	1943	1982	2011	2007	2002	1963	1919
JJA	1986	1923	1948	1949	1956	1959	1962
SON	1986	1996	1991	1989	1954	1950	1945
Full year	1989	1986	1974	1984	1959	1990	2002
				Storminess			
DJF	1915	1984	1936	1960	1910	1919	1900
MAM	1983	1981	1920	1908	1919	1922	1909
JJA	2012	1879	1927	1888	1986	1917	1956
SON	2000	1935	1872	1976	1916	1974	1896
Full year	1872	1927	1916	1930	1951	2000	2009

684 **Table 3**. Correlation between BI cyclone metrics and atmospheric circulation indices. BIBF denotes the blocking frequency
685 in the BI domain (50-60°N, 16°W-6°E); 20CR PC and station-based NAO indices are subscripted with $_{pc}$ and $_{station}$,
686 respectively. Correlations in **bold** are significantly different from zero at $p<0.05$, according to a two-tailed *t*-test.

Season	Cyclone metric	NAO_{pc}	$NAO_{station}$	GBI	BIBF
DJF	Counts	**-0.40**	**-0.20**	**0.33**	**-0.53**
	Intensity	**0.56**	**0.48**	**-0.48**	*0.05*
MAM	Counts	**-0.27**	*-0.11*	**0.25**	**-0.65**
	Intensity	**0.26**	**0.19**	**-0.26**	*0.05*
JJA	Counts	**-0.33**	*-0.09*	**0.21**	**-0.65**
	Intensity	*0.01*	*0.00*	*-0.08*	*0.02*
SON	Counts	*0.01*	*0.12*	*0.13*	**-0.68**
	Intensity	**0.29**	**0.23**	**-0.23**	**-0.18**

687

688 **Table 4**. Relative cyclone and blocking frequency for the BI domain in summer for 30-year normal periods (except 1991-
689 2012). Here blocking frequency is calculated according to the definition of the BIBF with percentages derived relative to the
690 long-term (1871– 2012) summer mean.

Period	Relative Cyclone Frequency (%)	Relative Blocking Frequency (%)
1871-1900	101.8	86.6
1901-1930	105.5	99.8
1931-1960	106.7	100.6
1961-1990	80.9	123.0
1991-2012	105.1	90.1

691

692

693

694

695 ## Figure captions

696 **Figure 1**. Panels **a** and **b** indicate the decadal mean standard deviation of daily-mean sea-level pressure amongst the 56
697 20CR ensemble members for the respective decades. To produce these fields, the standard deviation of the daily mean sea-
698 level-pressure was calculated across the 56 ensemble members at each grid cell. Time averages for these fields were then
699 calculated for each grid cell and respective decade. Panel **c** shows the data in the middle panel as a fraction of that plotted in
700 **a**. The larger the fraction, the less uncertainty has changed with time implying greater homogeneity in those regions.

701 **Figure 2.** Relationship between 20CR cyclone counts and total pure (left) and hybrid (right) cyclonic LWTs. Seasonal
702 correlation coefficients (multiplied by 100) between series are also shown. Solid black lines denote the 1:1 relationship.
703 'Cyclone days' is defined as the number of cyclones identified in the six-hourly grids, divided by 4 (to be consistent with the
704 once-daily LWT classification).

705 **Figure 3.** Correlation between gridded CRU TS3.21 precipitation and seasonal cyclone metrics. White areas over land
706 denote where correlations are insignificant (p>0.05). Upper and lower correlation coefficients (r) given in each panel are the
707 mean correlations for the whole domain (36.25°N to 69.75°N, 11.75°W to 19.75°E) and BI only, respectively.

708 **Figure 4.** Seasonal variations in cyclone metrics for the BI. All 56 ensemble members' six-hourly time series of cyclone
709 counts and intensity were convolved with a 31-day window (with weights equal to the reciprocal of window length). This
710 converts counts to a probability of at least one cyclone being present in the BI domain for the respective time of the year.
711 Storminess was calculated from these smoothed series, expressed as units of probability-weighted intensity; cyclone
712 intensity is in units of Laplacians of sea-level pressure. Smoothed series were averaged over all ensemble members and 142
713 years (i.e. 1871-2012) to generate the seasonal profiles. Shaded areas denote ± one standard error of the mean; tick marks
714 indicate the beginning of a month.

715 **Figure 5.** Mean cyclone counts by season. Bars denote ± one standard error in the ensemble mean for 30-year blocks (except
716 1991-2012).

717 **Figure 6.** Annual cyclone metrics by season and full year. Solid lines show the ensemble mean and shaded regions span the
718 range of the 56 ensemble members. Dotted lines are the 11-year moving average. Units of count are simply the number of
719 centres detected in the six-hourly grids, whilst intensity and storminess have units of Laplacians of mean sea-level pressure.

720 **Figure 7.** Decadal mean cyclone statistics by season expressed as a z-score averaged over all 56 20CR ensemble members.
721 Error bars indicate ± one standard deviation of the 56 decadal means. Numbers above/below the bars give the rank of the
722 decade for the respective metric and season.

723 **Figure 8.** Composite standardized anomalies (z-scores) in the 500 hPa geopotential height field for the years of exceptional
724 cyclone frequency (left) and intensity (right) (see Table 2). Grid cells with absolute z-scores less than 1 are white.

725 **Figure 9.** Correlation between blocking frequency (BITM) at each grid point and cyclone frequency (left) and intensity
726 (right) over the BI. Regions where the correlation is significantly different from zero at p <0.05 (according to a two-tailed t-
727 test) are coloured.

728 **Figure 10**. Left: Seasonal cycle of cyclone probability and blocking probability for the BI domain. The cyclone probability
729 curve is taken from Figure 4. The blocking curve is calculated via the same convolution procedure described in Figure 4
730 caption, and represents the probability of at least one grid cell being blocked in the BI domain. Right: Summer minus winter
731 blocking frequency (%) across the North Atlantic region, averaged over the full length of the 20CR.

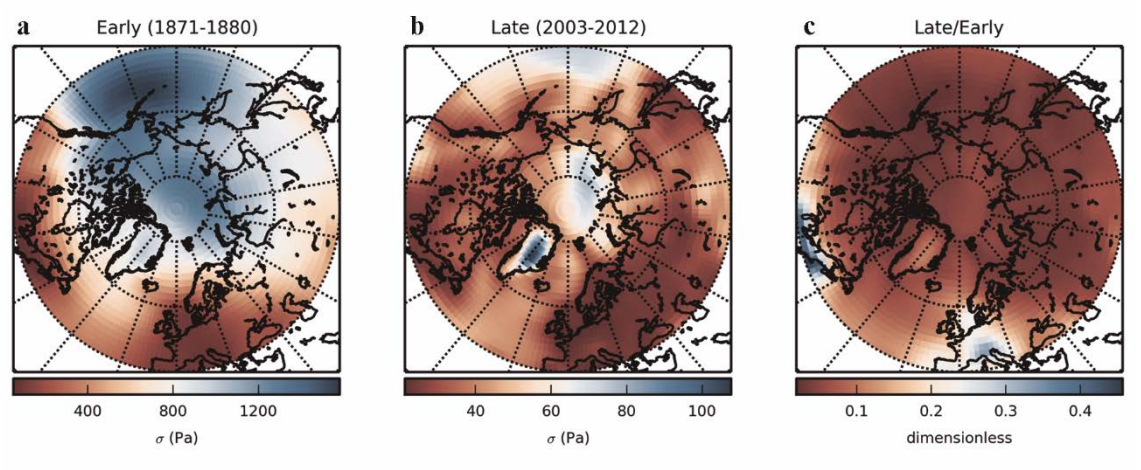

732

733 **Figure 4.**

734

735

736

737

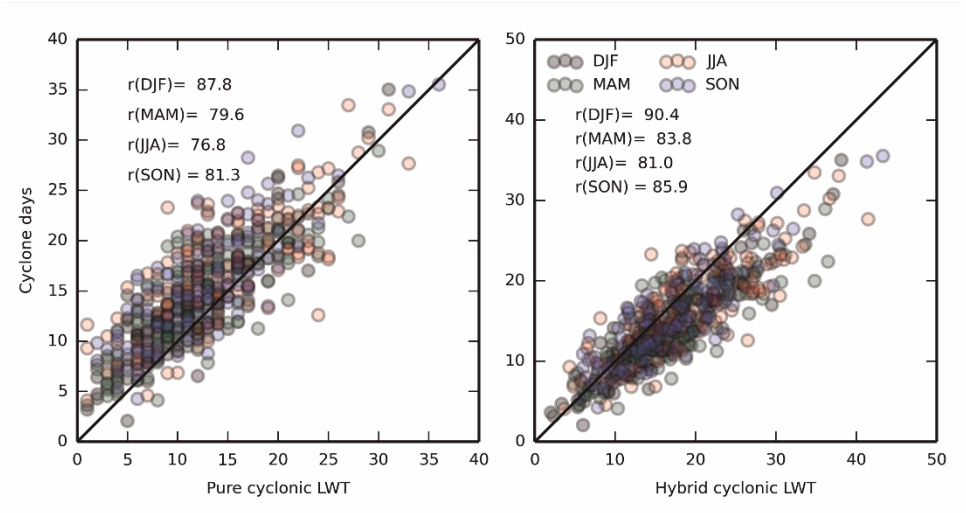

738

739 **Figure 5.**

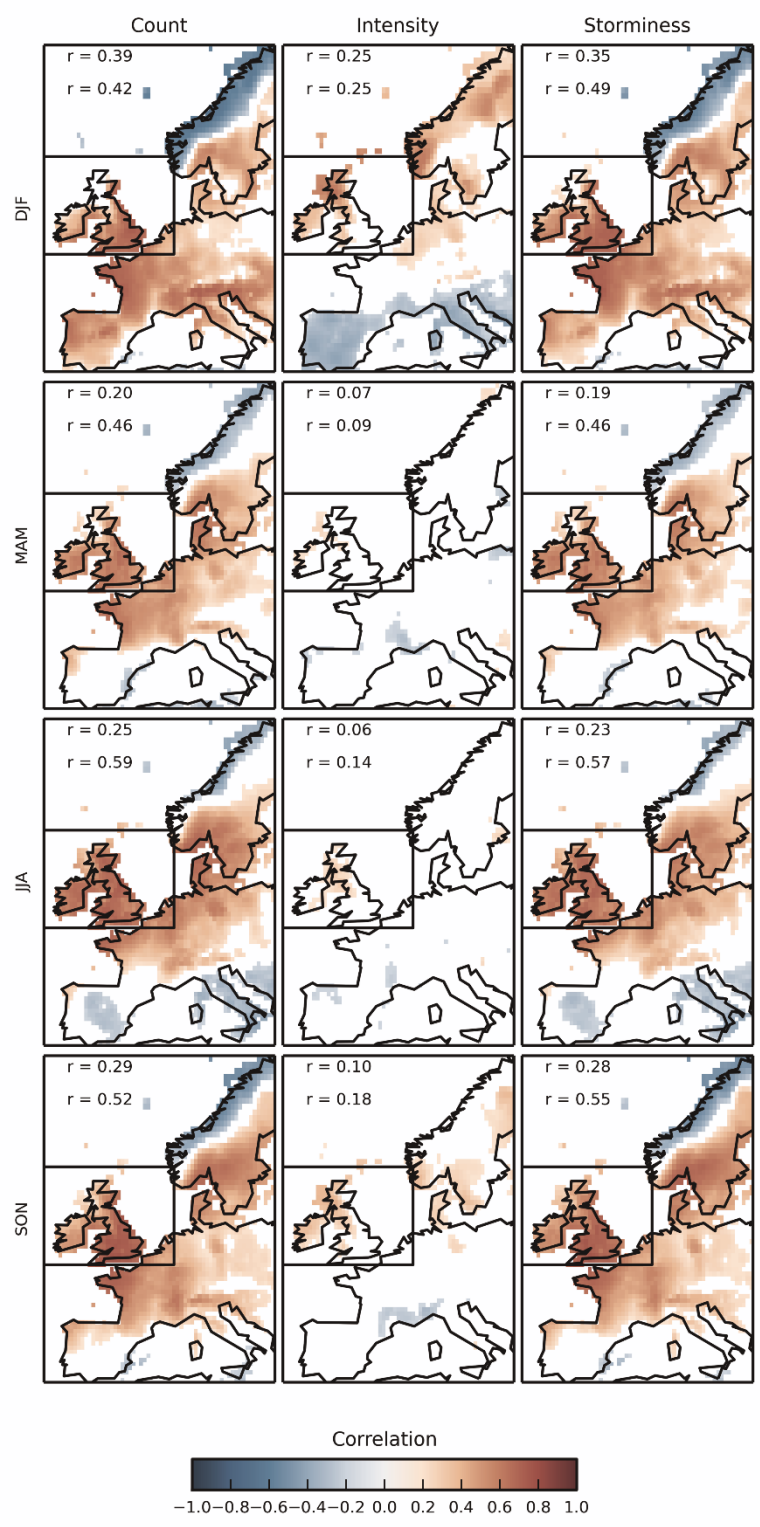

740

741 **Figure 6.**

742

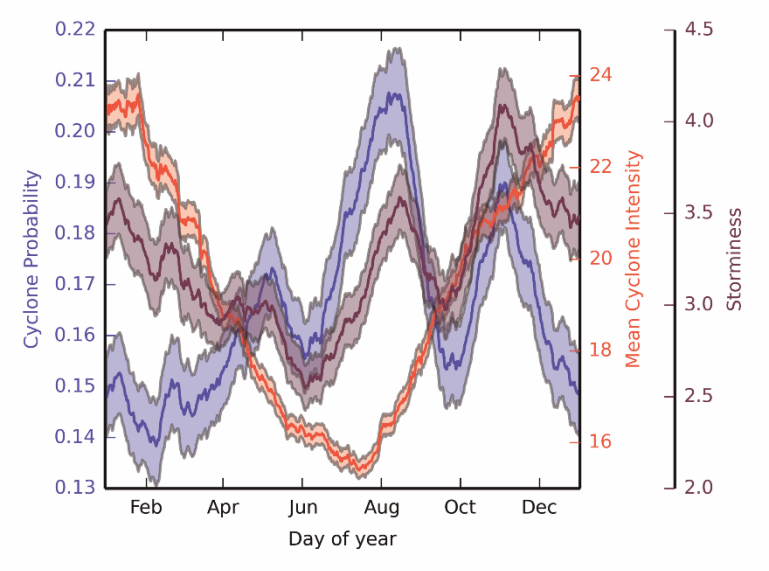

743

744 **Figure 4.**

745

746

747

748

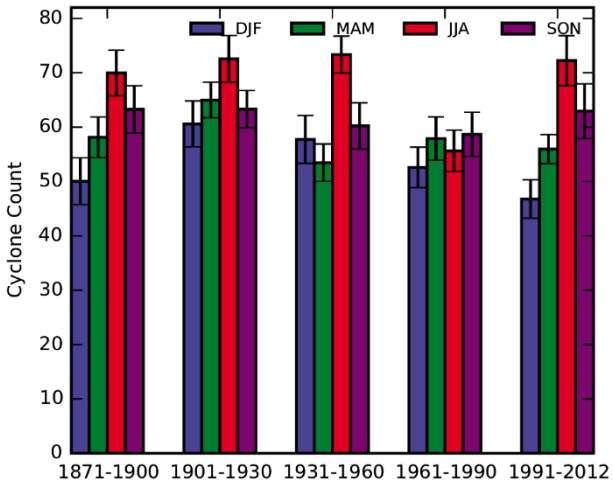

749

750 **Figure 5.**

751

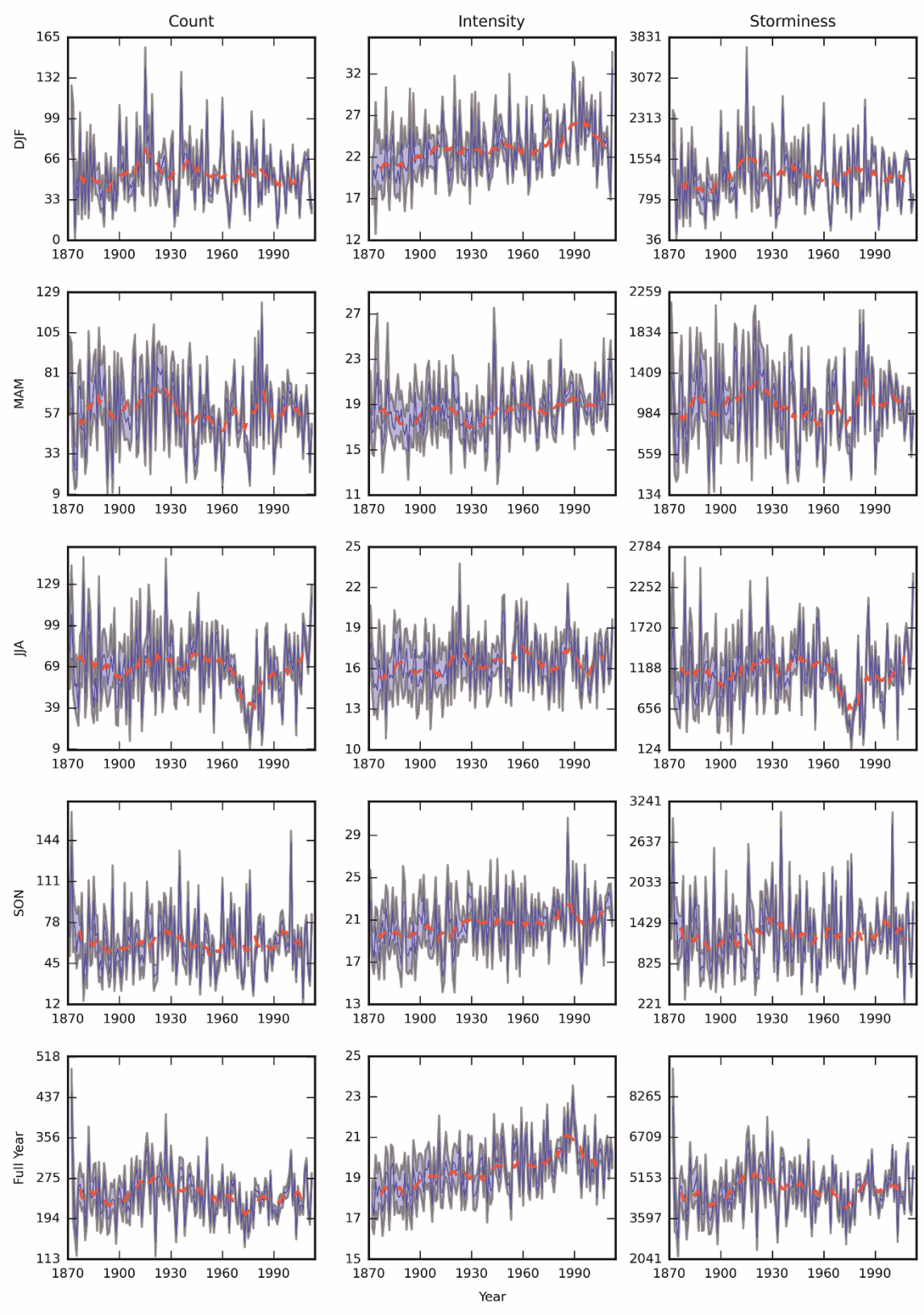

752

753 **Figure 6.**

754

755

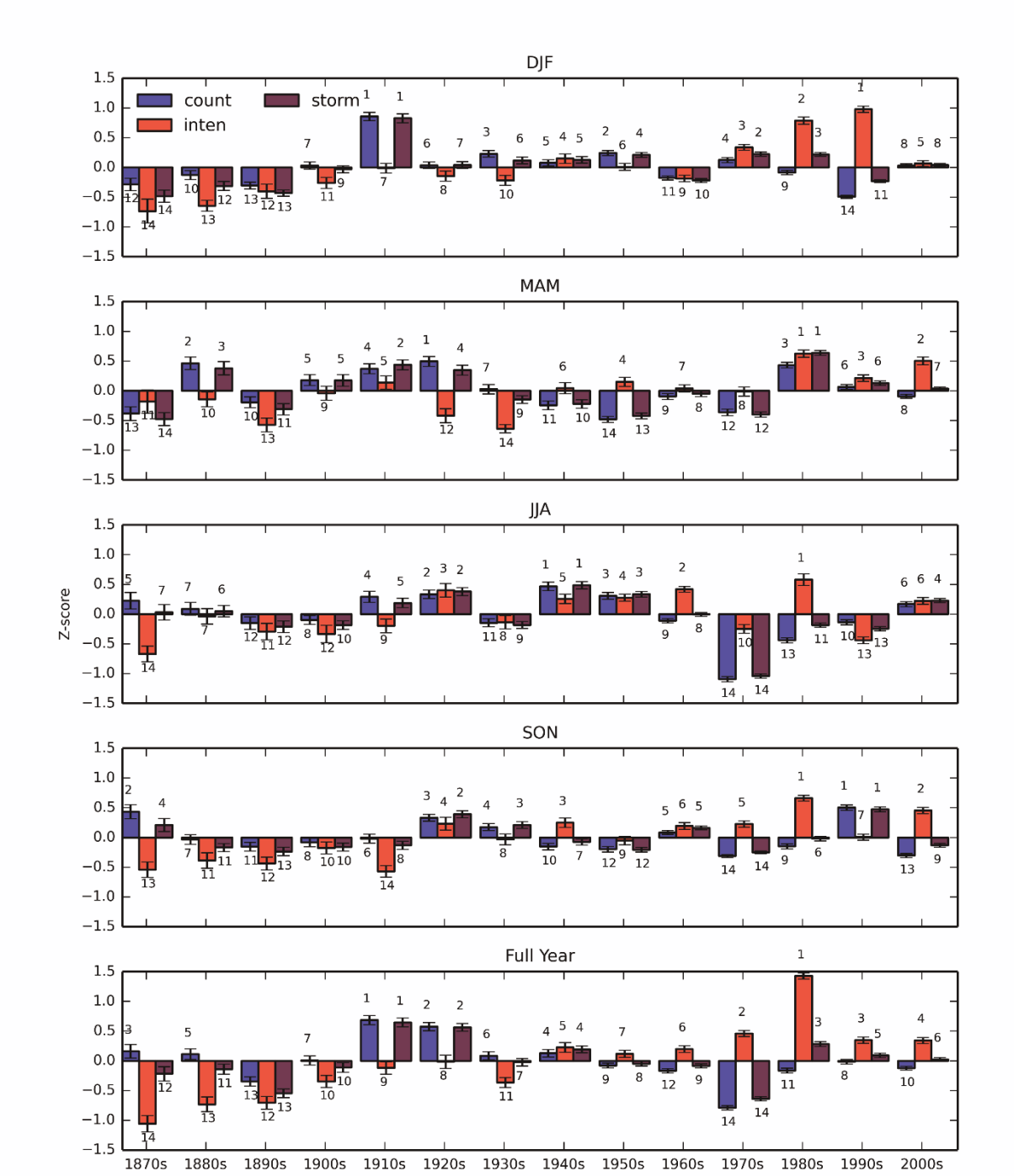
DJF
MAM
JJA
SON
Full Year
count
storm
inten
Z-score
1.5
1.0
0.5
0.0
−0.5
−1.0
−1.5
1870s
1880s
1890s
1900s
1910s
1920s
1930s
1940s
1950s
1960s
1970s
1980s
1990s
2000s

Figure 7.

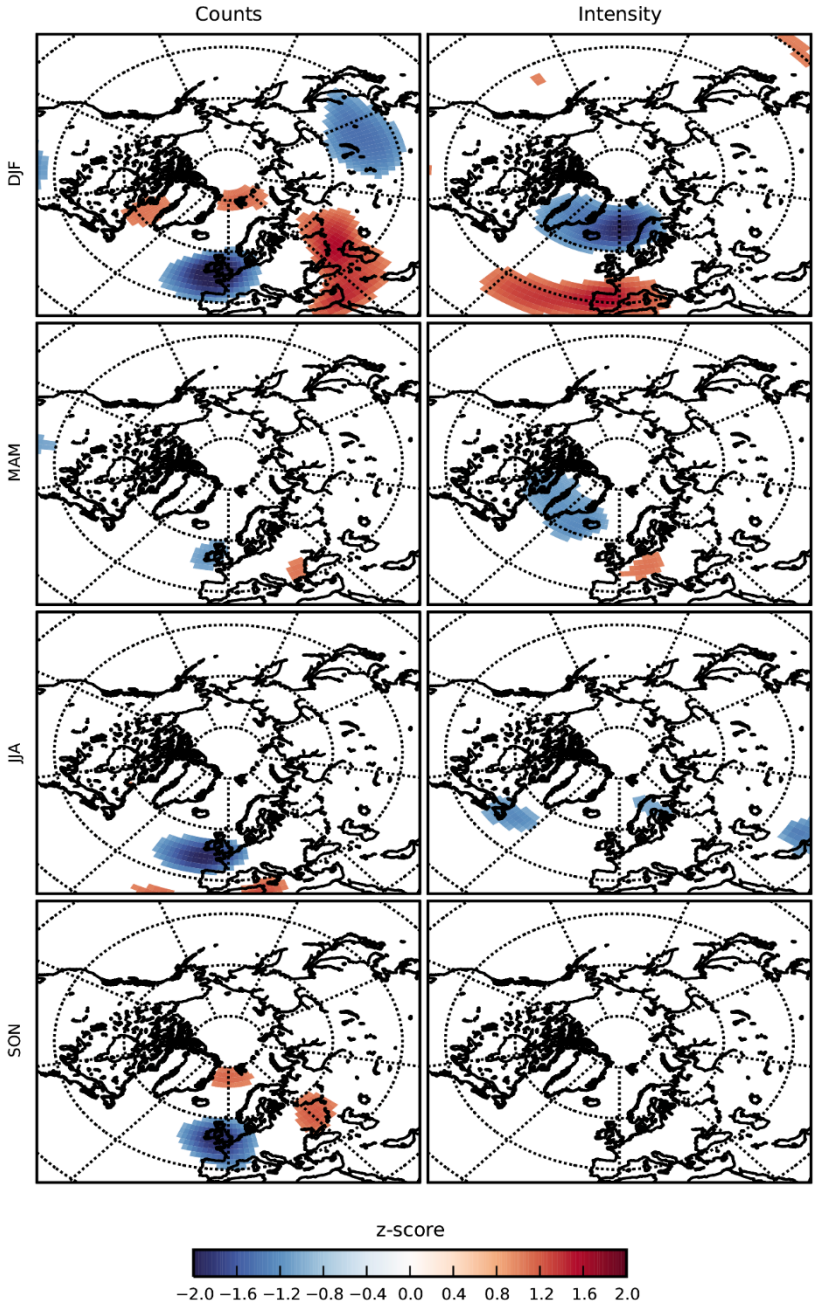

762

763 **Figure 8.**

764

765

766

767

768

769

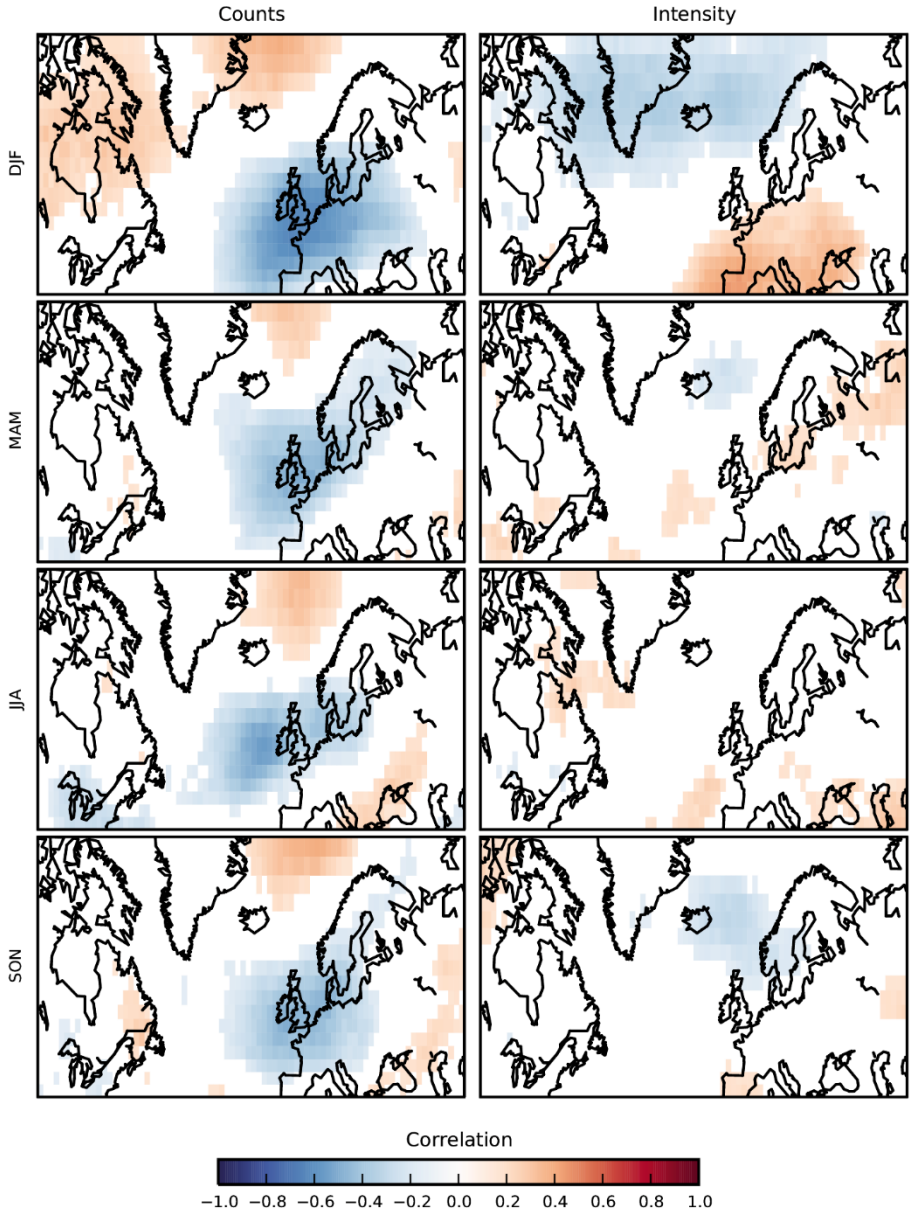
Counts
Intensity
DJF
MAM
JJA
SON
Correlation
−1.0 −0.8 −0.6 −0.4 −0.2 0.0 0.2 0.4 0.6 0.8 1.0

Figure 9.

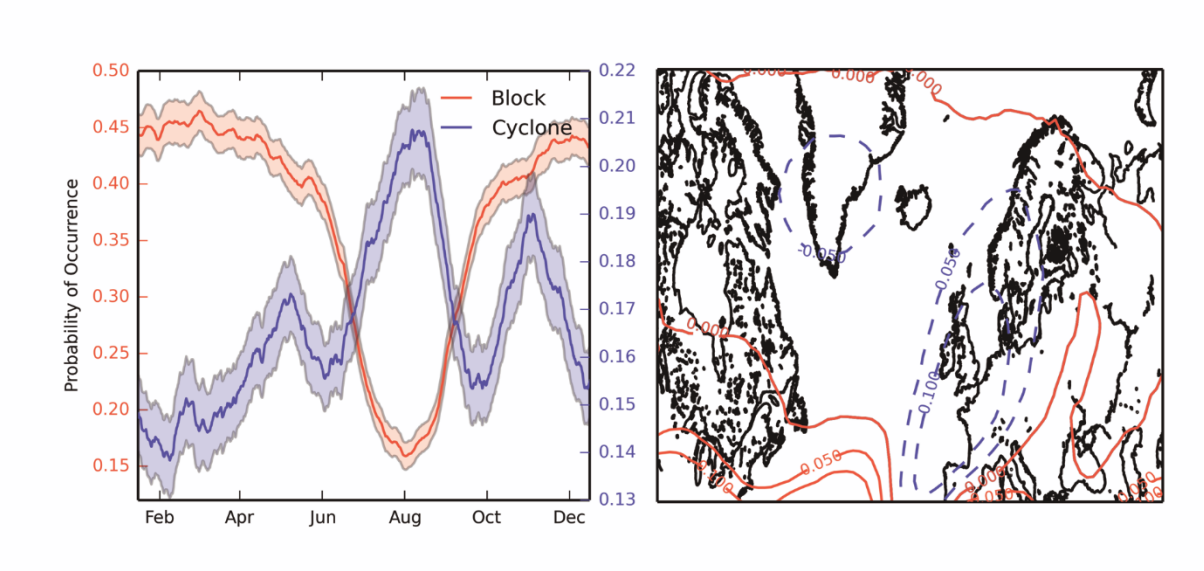

774

775 **Figure 10.**